
ParticleGS: Particle-Based Dynamics Modeling of 3D Gaussians for Prior-free Motion Extrapolation

Jinsheng Quan Chunshi Wang Yawei Luo ✉

Zhejiang University

Abstract

This paper aims to model the dynamics of 3D Gaussians from visual observations to support temporal extrapolation. Existing dynamic 3D reconstruction methods often struggle to effectively learn underlying dynamics or rely heavily on manually defined physical priors, which limits their extrapolation capabilities. To address this issue, we propose a novel dynamic 3D Gaussian Splatting prior-free motion extrapolation framework based on particle dynamics systems. The core advantage of our method lies in its ability to learn differential equations that describe the dynamics of 3D Gaussians, and follow them during future frame extrapolation. Instead of simply fitting to the observed visual frame sequence, we aim to more effectively model the gaussian particle dynamics system. To this end, we introduce a dynamics latent state vector into the standard Gaussian kernel and design a dynamics latent space encoder to extract initial state. Subsequently, we introduce a Neural ODEs-based dynamics module that models the temporal evolution of Gaussian in dynamics latent space. Finally, a Gaussian kernel space decoder is used to decode latent state at the specific time step into the deformation. Experimental results demonstrate that the proposed method achieves comparable rendering quality with existing approaches in reconstruction tasks, and significantly outperforms them in future frame extrapolation. Our code is available at <https://github.com/QuanJinSheng/ParticleGS>.

1 Introduction

Enabling machines to understand the spatiotemporal dynamics of a scene from just a few seconds of video and automatically infer the subsequent motion is crucial for applications like gaming, autonomous driving, and robotics [1, 2, 3]. Although existing methods [4, 5, 6, 7, 8, 9, 10] can reconstruct and render vivid 4D scenes, they primarily focus on reconstructing and rendering observed spatiotemporal sequences, without explicitly learning the dynamic evolution of the scene. As a result, they often struggle with extrapolating future frames.

Related work has addressed this issue by embedding physics knowledge into machine learning models [11, 12, 13, 14, 15, 16, 17, 18, 19]. Some approaches introduce explicit simulation frameworks (*e.g.*, Material Point Method [20], Quadratic Moving Least Squares [21]), simulating particle motion extrapolation by setting the forces on objects and properties [11, 22, 23]. Although subsequent methods learn material properties from video or video diffusion models, they still require manually specified external forces [14, 15, 16, 19, 24], which somewhat limits the flexibility of motion. Other approaches, such as those based on Physics-Informed Neural Networks (PINNs) [17], embed physical constraints directly into the learning process. For example, [13, 18] incorporates the Navier-Stokes equation from fluid dynamics to constrain the velocity field for future frame extrapolation. In addition, although there have been some pioneering works based on Neural Ordinary Differential Equations (Neural ODEs) [25] for learning dynamic [26, 27], none of them are capable of directly learning motion patterns from videos.

Preprint. Under review.

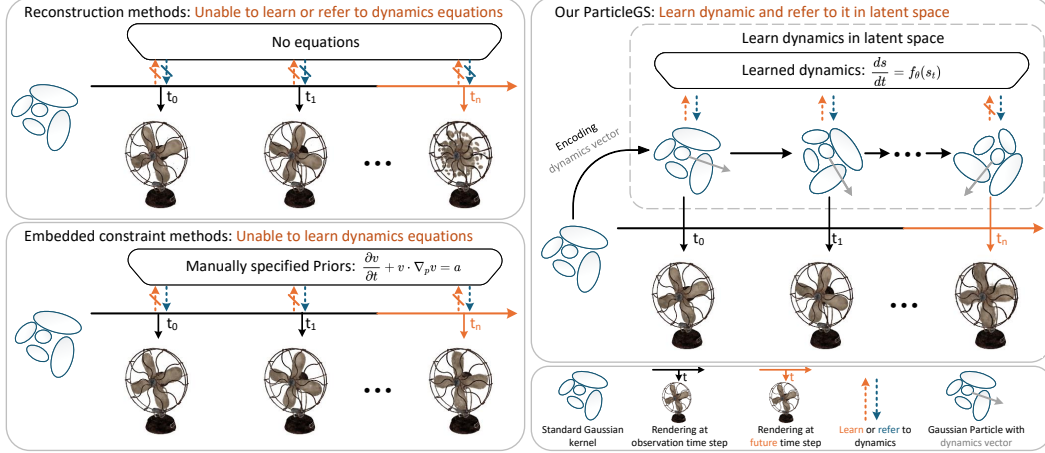


Figure 1: Differences between existing methods and ours. 1) Existing reconstruction methods are unable to learn or refer to dynamical laws; 2) Existing physics-informed methods can only refer to manually defined specific prior and cannot learn them automatically; 3) Our method introduces a latent dynamical space that automatically learns a parametric representation of the dynamics laws from observational data and refer to them in future predictions.

These limitations raise a core question: *Is it possible to learn the dynamics of evolving 3D scenes end-to-end, enabling extrapolation without relying on manually defined priors?* To address this question, we propose a novel dynamic 3D Gaussian Splatting prior-free Motion Extrapolation framework based on particle dynamics systems. Specifically, we observe a similarity between the Gaussian representation of dynamic 3D scenes and the evolution of particle trajectories in classical dynamics systems. Inspired by the modeling approach in dynamical systems, where a particle’s behavior is governed by a state vector that evolves over time, we introduce a latent dynamics state vector into the standard Gaussian kernel, transforming it into a Gaussian particle. A Gaussian particle not only encodes static attributes but also carries a latent state vector that describes its temporal behavior. Unlike traditional methods that reconstruct each frame independently [4, 5, 6, 7, 18, 8], our approach aims to learn the temporal evolution of the latent state, thereby enhancing generalization to future time steps. The core advantage of this approach lies in its ability to automatically learn a parametric representation of the underlying dynamics from observed data, leading to stable and consistent extrapolation capabilities. As shown in 1, this method offers a dual advantage. On one hand, unlike existing approaches that impose explicit physical constraints, the Neural ODEs-based method requires no prior knowledge about object categories, material properties, or dynamical equations. Instead, it learns the dynamics directly from video observations. On the other hand, compared to current reconstruction networks that often overfit to the training time window, our method follows the same learned differential equations during extrapolation, enabling it to generalize beyond the observed temporal range.

Specifically, we first propose a dynamic latent space encoder that encodes the initial latent state z_0 of each Gaussian particle, which is composed of both its local fine-grained features and the global features of the system. Then, to efficiently learn the evolution process of the particle system, we introduce a Neural ODE-based dynamics module that simulates the evolution of global features to the target time step, enabling the generation of latent states z_t at arbitrary time steps. Finally, we design a Gaussian kernel space decoder that decodes the temporally evolved latent state z_t into a deformed standard Gaussian kernel, enabling rendering of the dynamic scene at any given moment.

To the best of our knowledge, ParticleGS is currently the first end-to-end, general dynamic 3D extrapolation method that does not require any manually defined physical priors. To demonstrate the effectiveness of ParticleGS, we compare it with several state-of-the-art dynamic 3D reconstruction and extrapolation models. The contributions of this work can be summarized as follows:

- We treat the Gaussian representation of the 3D scene as a particle dynamics system by assigning an additional dynamics latent state dimension, which implicitly represents the dynamics state of each Gaussian particle and is updated from video motion information.

Therefore, there is no need to manually define priors such as object types, materials, forces, simulation frameworks, or dynamic equations.

- To update the latent state end-to-end from video motion information, we propose a Dynamics Latent Space Encoder to extract the latent state of standard Gaussian kernels. A Gaussian Kernel Space Decoder is used to decode deformation from the latent state, and a Neural ODE solver is used to model the evolution of the latent states over time.
- Numerical experiments on existing benchmarks show that our method achieves reconstruction performance on par with current state-of-the-art approaches, while outperforming them in future frame extrapolation.

2 Related Works

Dynamic 3D reconstruction. Neural Radiance Fields (NeRF) [28] is a key method for addressing the problem of 3D scene reconstruction. To extend its capability to model dynamic scenes, subsequent approaches commonly adopt time-varying deformation fields to achieve dynamic scene rendering. To improve the accuracy or efficiency of dynamic scene rendering, some methods decompose the input into planes [29, 7, 30, 31], while others introduce hash encoding [32, 9, 33]. Additionally, some works incorporate extra supervision for different modeling purposes [34, 35, 36]. However, the implicit representation of NeRF leads to issues such as slow training convergence and prominent geometric noise [16, 14]. Recently, 3D Gaussian Splatting (3DGS) [37] has attracted widespread attention due to its advantages in explicit geometric modeling and real-time rendering. Similar to the technical evolution of NeRF, dynamic 3DGS methods enhance modeling capability by extending static Gaussian point clouds with deformation fields [38, 4, 5, 39, 40, 8, 41]. However, existing methods generally focus on spatiotemporal interpolation tasks, and the lack of extrapolation ability limits their practicality in applications that require the prediction of future states. In this paper, we propose a time-evolution module based on NODE to learn the dynamic evolution of 3D scenes for extrapolation.

Scientific Machine Learning for dynamic 3D. Understanding physical laws is crucial for simulating and predicting 3D dynamic scenes [42, 43, 44, 45]. Scientific Machine Learning for 3D has made significant progress in recent years [46, 47]. Some works have incorporated physical equations into deep learning frameworks [17, 48, 49, 50], embedding equations such as the Navier-Stokes equations and elasticity mechanics to solve motion extrapolation [18, 13]. Although this approach performs well in certain scenes, it somewhat limits the capability for general scenarios, as the dynamics of complex scenes may not perfectly satisfy the embedded constraints. Meanwhile, an increasing number of studies are introducing physical simulation engines into deep learning frameworks [14, 16, 51, 52, 53, 54, 55]. Since the physical engines provide strong priors, physical extrapolation can often be achieved by manually setting external forces. However, the manual setting of forces may lead to suboptimal solutions, limiting the flexibility of the model. Some methods combining Graph Neural Networks (GNNs) have also started to emerge in the field of physical simulation [56, 57, 58]. The approach closest to our work is GaussianPrediction [56], which proposes a multi-stage model to learn time-independent neighborhood relationships and achieve extrapolation by predicting keypoint dynamics. Although it has achieved good results, the inability of GNNs to represent system evolution over time limits the accuracy of their extrapolation. In contrast, NODE-based approaches have attracted attention due to their ability to learn the dynamic differential equations of time series [25]. However, existing methods are unable to predict future frames in an end-to-end manner [26, 27]. In this paper, our method directly learns the dynamics from multi-view videos without relying on manually specified physical priors.

3 Preliminary

3D Gaussian Splatting (3DGS) is an efficient and high-quality rendering method for static 3D scenes [37]. This method represents the entire scene by explicitly modeling a set of 3D Gaussian kernels with attributes, where each Gaussian kernel is defined as $k = \{\mu, \Sigma, \alpha, \mathbf{c}\}$. Here, μ denotes the position of the Gaussian kernel in 3D space, Σ is the covariance matrix describing the shape and orientation of the Gaussian, α is the opacity, and \mathbf{c} is the RGB color vector.

To improve optimization efficiency, the covariance matrix Σ is decomposed into a rotation R and a scaling S . During rendering, each 3D Gaussian is projected onto the image plane. Let V be the view matrix transforming from world coordinates to camera coordinates, and J be the Jacobian matrix of the projection transformation. Then, the 2D covariance matrix Σ' in image space is:

$$\Sigma' = JV\Sigma V^\top J^\top, \quad \Sigma = RSS^\top R^\top. \quad (1)$$

The image is generated through point-based volume rendering. For a pixel p on the image plane, its final color $C(p)$ can be expressed as:

$$C(p) = \sum_{i \in \mathcal{N}_p} T_i \alpha_i \mathbf{c}_i, \quad \alpha_i = \sigma_i \cdot \exp\left(-\frac{1}{2}(p - \mu_i)^\top \Sigma_i'^{-1}(p - \mu_i)\right), \quad T_i = \prod_{j=1}^{i-1} (1 - \alpha_j). \quad (2)$$

Here, σ_i controls the intensity of the Gaussian, μ_i is the projection center of the Gaussian kernel on the image plane, and T_i represents the transmittance of the Gaussian, computed from the accumulated opacity of preceding Gaussians.

4 Methodology

4.1 Problem Formulation and Overview

In this paper, we transform the standard 3D Gaussian kernel k into a Gaussian particle $s_t = \{(k, z_t) \mid k \in \mathbb{R}^n, z_t \in \mathbb{R}^m\}$, which enable us to model the motion of Gaussian kernels with particle dynamics. Here, $k \in \mathbb{R}^n$ represents a standard Gaussian kernel in an n -dimensional space, and $z_t \in \mathbb{R}^m$ denotes vector of the Gaussian particle at time t in dynamics latent space, which implicitly describes its dynamic evolution through m parameters.

Formally, given a set of viewpoints $\{v\}$ and the corresponding visual observation sequences $\{I_t^v\}_{t=1}^{T'}$, the objective is to learn a dynamical model $\frac{ds}{dt} = f_\theta(s_t)$ that captures the evolution of a 3D Gaussian particle system. The model should minimize the rendering loss between the predicted future sequences $\{\hat{I}_t^v\}_{t=T'}^T = \mathcal{R}(s_t)_{t=T'}^T$ and the ground-truth sequences $\{I_t^v\}_{t=T'}^T$. Here, s_t represents the Gaussian particle evolved to time t by the dynamics model, and \mathcal{R} is a differentiable renderer.

Importantly, our goal is to predict the most likely future video sequence given the past observations $\{I_t^v\}_{t=1}^{T'}$, that is:

$$\{\hat{I}_t^v\}_{t=T'}^T = \arg \max_{\{I_t^v\}} p(\{I_t^v\}_{t=T'}^T \mid \{I_t^v\}_{t=1}^{T'}), \quad (3)$$

rather than being based on the conditional property d , such as $\arg \max_{\{I_t^v\}} p(\{I_t^v\}_{t=T'}^T \mid \{I_t^v\}_{t=1}^{T'}, d)$. For example, when observing a man walking along a road, we aim to predict that he will continue walking rather than sit down by a condition $d = \text{"A man suddenly sits down"}$.

The overview of our framework is illustrated in Figure 4.1 and consists of three modules: a dynamics latent space encoder, a dynamics evolution module and a Gaussian kernel space decoder.

4.2 Dynamics Latent Space Encoder

Since motion in the natural world often affects entire objects or regions, it corresponds to the overall movement trend of Gaussian particles. In contrast, information such as color and texture tends to change rapidly in space, corresponding to fine local features. Therefore, we extract multi-scale feature as the initial latent state $z_0 = (g_0, l)$ for each Gaussian particle, where $g_0 \in \mathbb{R}^G$ represents the global features of Gaussian particles system at the initial state, and $l \in \mathbb{R}^{N \times L}$ denotes the local features, with N being the number of Gaussian particles, G the dimensionality of the global features, and L the dimensionality of the local features.

Local Feature Encoding. Following the encoding method used in InstantNGP [32], we apply a multi-resolution hash encoding to the mean $\mu = (x, y, z)$ of the standard Gaussian kernel to obtain the local features l . We define L resolution levels, ranging from coarse to fine within the range $[N_{\min}, N_{\max}]$, where the resolution at level i is:

$$N_i = \lfloor N_{\min} \cdot b^i \rfloor, \quad b = \exp\left(\frac{\ln N_{\max} - \ln N_{\min}}{L - 1}\right). \quad (4)$$

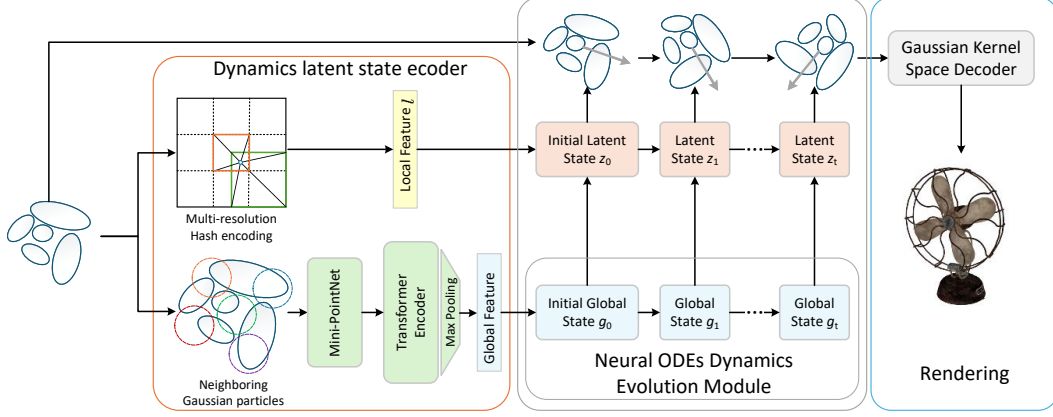


Figure 2: Overview. The dynamics latent space encoder extracts the initial latent state $z_0 = (g_0, l)$, where l represents fine-grained local features for each Gaussian, and g_0 denotes the global feature shared across the particle system. The Neural ODE dynamics evolution module predicts the latent state $z_t = (g_t, l)$ of the system evolved to a specific time step. The Gaussian Kernel Space Decoder decodes the latent state into deformations of standard Gaussians for rendering.

Each level i is associated with a hash table $T_i \in \mathbb{R}^{M \times F}$, where M is the table size and F the feature dimension. A hash function $h_i : \mathbb{Z}^d \rightarrow \{0, 1, \dots, M - 1\}$ maps grid vertex coordinates $\mathbf{g} \in \mathbb{Z}^d$ to a hash index:

$$h_i(\mathbf{g}) = \left(\bigoplus_{i=1}^d g_i \pi_i \right) \bmod M. \quad (5)$$

Here, d is the input dimension, π_i are large prime numbers, and \oplus denotes the bitwise XOR operation.

Global Feature Encoding. Inspired by PointNet [59] and Point-BERT [60], we encode the global feature g_0 using a self-attention mechanism followed by max pooling. For each $\mu = (x, y, z)$, we first apply farthest point sampling (FPS) to select a set of center points, then use the k-nearest neighbors (KNN) algorithm to find the neighboring points for each center, forming groups of neighboring Gaussian particles. Each group is encoded into a neighborhood feature using a mini-PointNet. Neighborhood-based encoding methods have been proven effective in several scientific machine learning applications [15, 12]. These neighborhood features are then passed through a self-attention module to enhance context awareness and finally compressed into the global feature g_0 via max pooling. To improve efficiency, we only recompute FPS and KNN groupings during clone, split, delete or every 500 training iterations.

4.3 Neural ODEs Dynamics Evolution Module

Neural ODEs are inherently well-suited for modeling systems with continuously evolving states over time. Their key advantage lies in learning the differential equation $\frac{dz(t)}{dt} = f_\theta(z_t, t)$ directly, where the rate of change of a variable depends solely on its current state and time. This property allows the model to autonomously discover underlying dynamics from data, without relying on prior physical assumptions such as fluid or rigid body mechanics.

To enable the model to learn physical motion patterns without being influenced by spatial details, we introduce a Neural ODE-based dynamics evolution module to model the continuous evolution of a Gaussian particle system in the dynamics latent space. After obtaining the initial latent feature z_0 , the Neural ODE predicts the evolution at a target time step by estimating the differential equation of the latent state:

$$z_t = (g_t, l), \quad g_t = g_0 + \int_0^t f_\theta(g_\tau, \tau) d\tau = \text{ODESolve}(f_\theta, g_0, 0, t), \quad (6)$$

where g_0 is the initial global state, z_t is the latent state at time step t , f_θ is the parameterized dynamics function, and ODESolve is the standard Neural ODE solver. In our ParticleGS, the RK4 method can be perfectly employed as a numerical integration solver.

4.4 Gaussian Kernel Space Decoder

Since the motion of most physical systems exhibits locally structured patterns rather than purely random displacements, we propose a decoder based on affine transformations to better capture these regularities. In contrast to prior approaches that directly regress displacement vectors [4, 5], our design encourages the model to learn interpretable and physically plausible motion fields aligned with the underlying structure. For the latent state at a specific time step z_t , we design independent multi-head decoders to predict the transformation components of particles:

$$\mu' = \mu + A\mu + b, \quad R' = R + \Delta R, \quad S' = S + \Delta S, \quad D(z_t) = \{A, b, \Delta R, \Delta S\}, \quad (7)$$

where $A \in \mathbb{R}^{3 \times 3}$ is the transformation matrix and $b \in \mathbb{R}^{3 \times 1}$ is the translation vector. Gaussian Kernel Space Decoder decodes affine deformations for each Gaussian kernel from a naturally continuous dynamics latent space. Therefore, the decoding process not only preserves the local structural consistency of similar Gaussians but also enables flexible modeling of diverse motion patterns. See the Appendix for implementation details.

4.5 Optimizing ParticleGS

Similar to 3DGS [37], we compute the \mathcal{L}_1 loss and D-SSIM loss between the rendered image and the ground-truth image at each time step:

$$\mathcal{L} = (1 - \lambda)\mathcal{L}_1 + \lambda\mathcal{L}_{SSIM}, \quad (8)$$

where λ is a hyperparameter that balances the two losses. Following existing works [4, 5, 8], we first warm up the standard Gaussian kernels, and then jointly optimize them with the network.

5 Experiments

5.1 Experimental Setup

Datasets. It is important to note that existing datasets (*e.g.*, D-NeRF datasets [6], HyperNeRF datasets [61]) are primarily designed for novel view synthesis tasks. Simply splitting the later portion of a sequence as the test set does not align with the natural video dynamics defined as definition 3. Therefore, we primarily adopt two benchmarks specifically designed for dynamic extrapolation. Specifically, NVFi introduces two synthetic datasets: the Dynamic Object dataset, which includes 6 objects exhibiting various types of motion such as rigid body motion and elastic deformation; and the Dynamic Indoor Scene dataset, which contains 4 scenes with multiple moving objects. For datasets provided by NVFi, we follow their original setup: data with timestamps less than 0.75 are used for training, while data with timestamps greater than 0.75 are used to evaluate extrapolation performance. Due to the relatively sparse camera viewpoints in the NVFi datasets, most of the test data with timestamps less than 0.75 comes from novel views, which may result in the extrapolation metrics outperforming the reconstruction metrics.

Additionally, we carefully select the PanopticSports dataset from Dynamic 3D Gaussians [38] for evaluation. This dataset is based on real motion capture data and is characterized by complex and fast movements. To ensure the motion remains predictable, we use data with timestamps less than or equal to 0.9 for training and evaluating reconstruction quality, and data with timestamps greater than 0.9 for evaluating extrapolation quality.

Baselines. We select two categories of methods as baselines: 1) State-of-the-art (SOTA) reconstruction methods: HexPlane [7] and TiNeuVox [9] are NeRF-based rendering approaches, while 4D-GS [5], DeformGS [4], and Grid4D [8] are reconstruction methods based on 3D Gaussian Splatting. 2) SOTA extrapolation: NVFi [18] is a PINN-based method that achieves extrapolation by embedding the Navier-Stokes equations as physical constraints. GaussianPrediction [56] is a GCN-based method that performs frame extrapolation by learning time-invariant neighborhood relations and using keypoint-driven motion prediction. All methods are conducted on a single RTX 4090.

Metrics. In this paper, we primarily report PSNR, SSIM, and LPIPS to evaluate the quality of frame extrapolation. However, similar to the perspective in NVFi [18], since the extrapolation metrics can be affected by the quality of the reconstruction process, an algorithm with perfect reconstruction but incorrect dynamics may outperform another with more accurate dynamics but less precise reconstruction in terms of metrics. Therefore, we also report reconstruction metrics as a reference.

Table 1: Quantitative results of all methods on reconstruction and extrapolation on the Dynamic Objects Dataset. The color of each cell shows the **best** and the **second best**.

Method	Shark						Whale					
	Reconstruction			Extrapolation			Reconstruction			Extrapolation		
	PSNR	SSIM	LPIPS	PSNR	SSIM	LPIPS	PSNR	SSIM	LPIPS	PSNR	SSIM	LPIPS
HexPlane	22.736	0.956	0.064	24.180	0.962	0.041	24.684	0.976	0.049	24.075	0.964	0.049
TiNeuVox	19.592	0.951	0.058	16.683	0.933	0.096	21.281	0.969	0.052	20.671	0.945	0.063
4D-GS	39.242	0.995	0.009	22.966	0.965	0.048	40.251	0.996	0.005	22.649	0.964	0.052
DeformGS	40.492	0.995	0.008	29.159	0.966	0.022	42.475	0.996	0.004	26.666	0.959	0.027
Grid4D	40.752	0.995	0.007	30.904	0.966	0.021	42.666	0.996	0.004	28.246	0.967	0.020
NVFi	31.374	0.982	0.035	28.649	0.979	0.033	30.778	0.984	0.025	25.529	0.977	0.029
GSPrediction	40.015	0.995	0.010	30.280	0.971	0.032	39.540	0.996	0.005	25.596	0.965	0.046
ParticleGS(Ours)	39.961	0.995	0.008	38.167	0.984	0.010	40.298	0.995	0.005	33.604	0.983	0.010

Method	Fan						Telescope					
	Reconstruction			Extrapolation			Reconstruction			Extrapolation		
	PSNR	SSIM	LPIPS	PSNR	SSIM	LPIPS	PSNR	SSIM	LPIPS	PSNR	SSIM	LPIPS
HexPlane	18.424	0.842	0.190	19.998	0.887	0.106	21.814	0.917	0.149	23.667	0.931	0.082
TiNeuVox	15.775	0.855	0.189	21.307	0.919	0.081	23.088	0.949	0.084	20.801	0.925	0.071
4D-GS	34.993	0.976	0.017	23.863	0.953	0.041	37.262	0.992	0.006	22.951	0.941	0.049
DeformGS	38.083	0.973	0.026	24.473	0.930	0.047	38.435	0.992	0.005	23.186	0.934	0.037
Grid4D	37.031	0.967	0.030	26.720	0.941	0.044	38.488	0.992	0.006	25.696	0.942	0.033
NVFi	27.748	0.953	0.059	27.347	0.957	0.054	26.889	0.955	0.051	26.861	0.955	0.053
GSPrediction	34.864	0.976	0.020	20.747	0.935	0.054	36.191	0.992	0.004	22.018	0.939	0.043
ParticleGS(Ours)	38.831	0.976	0.023	34.131	0.968	0.027	38.537	0.993	0.004	34.954	0.983	0.006

Method	Fallingball						Bat					
	Reconstruction			Extrapolation			Reconstruction			Extrapolation		
	PSNR	SSIM	LPIPS	PSNR	SSIM	LPIPS	PSNR	SSIM	LPIPS	PSNR	SSIM	LPIPS
HexPlane	19.754	0.816	0.215	20.166	0.906	0.130	22.099	0.953	0.080	22.422	0.954	0.061
TiNeuVox	24.323	0.894	0.167	20.474	0.940	0.098	17.611	0.946	0.076	17.139	0.947	0.070
4D-GS	20.310	0.851	0.157	21.476	0.930	0.101	38.889	0.995	0.006	20.066	0.956	0.077
DeformGS	17.736	0.830	0.156	26.384	0.945	0.060	47.034	0.996	0.004	27.109	0.944	0.034
Grid4D	19.119	0.821	0.153	24.926	0.925	0.069	47.443	0.997	0.004	29.551	0.953	0.290
NVFi	34.900	0.969	0.068	27.013	0.966	0.074	24.648	0.970	0.044	25.529	0.973	0.040
GSPrediction	24.549	0.910	0.154	16.790	0.830	0.238	43.290	0.997	0.002	23.495	0.952	0.075
ParticleGS(Ours)	21.047	0.861	0.201	27.558	0.947	0.057	47.118	0.997	0.004	36.932	0.982	0.013

Table 2: Quantitative results of all methods on reconstruction and extrapolation on the Dynamic Indoor Scene Dataset. The color of each cell shows the **best** and the **second best**.

Method	Gnome House						Chessboard					
	Reconstruction			Extrapolation			Reconstruction			Extrapolation		
	PSNR	SSIM	LPIPS	PSNR	SSIM	LPIPS	PSNR	SSIM	LPIPS	PSNR	SSIM	LPIPS
HexPlane	18.060	0.419	0.650	23.341	0.601	0.530	18.054	0.515	0.617	22.034	0.680	0.500
TiNeuVox	24.644	0.663	0.385	21.359	0.665	0.357	23.847	0.698	0.392	20.088	0.676	0.408
4D-GS	18.104	0.722	0.542	19.995	0.736	0.452	19.465	0.793	0.447	20.209	0.816	0.375
DeformGS	21.855	0.611	0.341	22.728	0.731	0.196	20.688	0.659	0.443	20.484	0.773	0.280
Grid4D	22.418	0.588	0.360	21.185	0.696	0.258	21.545	0.667	0.437	19.713	0.741	0.331
NVFi	16.857	0.435	0.687	24.087	0.615	0.546	17.515	0.551	0.651	22.571	0.672	0.539
GSPrediction	16.113	0.556	0.632	20.098	0.641	0.371	17.665	0.651	0.470	20.033	0.724	0.317
ParticleGS(Ours)	24.481	0.639	0.323	31.167	0.843	0.160	23.857	0.698	0.363	29.344	0.869	0.185

Method	Factory						Dining Table					
	Reconstruction			Extrapolation			Reconstruction			Extrapolation		
	PSNR	SSIM	LPIPS	PSNR	SSIM	LPIPS	PSNR	SSIM	LPIPS	PSNR	SSIM	LPIPS
HexPlane	19.109	0.479	0.637	24.266	0.677	0.470	16.687	0.516	0.601	23.127	0.725	0.395
TiNeuVox	24.857	0.705	0.346	22.467	0.747	0.292	21.476	0.658	0.368	20.529	0.768	0.276
4D-GS	19.256	0.763	0.518	20.948	0.800	0.387	20.445	0.797	0.345	20.845	0.841	0.276
DeformGS	21.703	0.621	0.376	23.471	0.787	0.196	15.832	0.488	0.621	21.244	0.784	0.258
Grid4D	21.822	0.631	0.377	22.119	0.765	0.235	16.407	0.475	0.595	19.516	0.741	0.313
NVFi	18.889	0.503	0.655	25.415	0.690	0.496	15.206	0.485	0.681	22.790	0.711	0.428
GSPrediction	17.388	0.588	0.609	21.723	0.713	0.308	13.451	0.546	0.688	18.214	0.679	0.374
ParticleGS(Ours)	25.028	0.780	0.244	33.568	0.914	0.104	18.139	0.516	0.544	25.010	0.809	0.253

Table 3: Quantitative results of all methods on reconstruction and extrapolation on the PanopticSports Dataset. The color of each cell shows the **best** and the **second best**.

Method	Boxes						Juggle					
	Reconstruction			Extrapolation			Reconstruction			Extrapolation		
	PSNR	SSIM	LPIPS	PSNR	SSIM	LPIPS	PSNR	SSIM	LPIPS	PSNR	SSIM	LPIPS
Grid4D	31.926	0.938	0.202	26.023	0.901	0.228	31.486	0.935	0.211	22.904	0.887	0.265
GSPrediction	28.353	0.929	0.135	26.612	0.913	0.154	29.337	0.935	0.138	24.316	0.920	0.166
ParticleGS(Ours)	30.271	0.943	0.183	27.012	0.920	0.204	29.297	0.939	0.126	25.158	0.924	0.225

Method	Tennis						Football					
	Reconstruction			Extrapolation			Reconstruction			Extrapolation		
	PSNR	SSIM	LPIPS	PSNR	SSIM	LPIPS	PSNR	SSIM	LPIPS	PSNR	SSIM	LPIPS
Grid4D	29.406	0.925	0.231	24.911	0.892	0.261	28.963	0.911	0.249	21.616	0.840	0.323
GSPrediction	27.304	0.923	0.168	26.133	0.917	0.178	27.257	0.912	0.185	24.234	0.891	0.209
ParticleGS(Ours)	28.086	0.931	0.210	26.084	0.918	0.234	26.903	0.917	0.230	24.535	0.894	0.262

Method	Softball						Basketball					
	Reconstruction			Extrapolation			Reconstruction			Extrapolation		
	PSNR	SSIM	LPIPS	PSNR	SSIM	LPIPS	PSNR	SSIM	LPIPS	PSNR	SSIM	LPIPS
Grid4D	29.142	0.926	0.236	24.029	0.890	0.273	26.862	0.897	0.278	21.990	0.829	0.342
GSPrediction	26.826	0.927	0.156	25.328	0.920	0.173	25.465	0.899	0.214	23.570	0.879	0.235
ParticleGS(Ours)	27.592	0.934	0.205	25.514	0.920	0.231	25.305	0.905	0.248	23.570	0.878	0.278

Table 4: Quantitative ablation results on the NVFi dataset. The color of each cell shows the **best**.

Method	Dynamic Object Dataset						Dynamic Indoor Scene Dataset					
	Reconstruction			Extrapolation			Reconstruction			Extrapolation		
	PSNR	SSIM	LPIPS	PSNR	SSIM	LPIPS	PSNR	SSIM	LPIPS	PSNR	SSIM	LPIPS
w/o Latent Space	17.644	0.946	0.069	14.133	0.924	0.099	14.793	0.502	0.556	15.497	0.568	0.458
w/o Neural ODE	37.518	0.969	0.041	33.790	0.970	0.024	22.278	0.625	0.392	28.658	0.817	0.191
w/o Affine Deformations	37.575	0.969	0.041	33.886	0.970	0.024	22.584	0.654	0.369	29.317	0.844	0.176
PartialGS(Ours)	37.632	0.969	0.041	34.224	0.974	0.021	22.876	0.658	0.369	29.772	0.859	0.176

5.2 Comparisons with Prior Work

Quantitative comparisons on synthetic dataset. Tables 1 and 2 present the quantitative metrics on dynamic object and indoor scene datasets, respectively. It is worth noting that ParticleGS achieves ~ 0.1 higher PSNR than Grid on the "Fan" and "Telescope" datasets. The main motion in these two datasets is rotation, which means that while the displacement of individual Gaussian particles exhibits high-frequency variation, the overall motion follows a clear and structured pattern. Since our method models global latent features, it is able to produce better results. In the "Fallingball" and "Indoor Scene" datasets, 3DGS-based methods show a notable drop in reconstruction quality due to sparse viewpoints, which often cause inaccurate geometry. ParticleGS, however, achieves ~ 2.0 higher PSNR. This is partly because our method aligns more closely with physical principles, making it difficult for incorrect geometry to reduce the loss through unrealistic motion, thereby leading to the optimization of a more accurate geometric structure.

Quantitative comparisons on real-world dataset. Table 3 presents the quantitative metrics on real-world datasets. GSPrediction performs better on the PanopticSports dataset than on synthetic datasets, primarily because it learns a time-independent neighborhood relationship, which effectively acts like a rigid-body constraint. This allows it to perform well for short-term motion. Nevertheless, our method still achieves ~ 0.3 higher PSNR on average than GSPrediction in the extrapolation task on PanopticSports. Additionally, in the reconstruction task on the Boxes dataset, although our method's PSNR is ~ 1.7 lower than that of Grid4D, it achieves a 0.005 higher SSIM and a 0.019 lower LPIPS. Similar trends are observed across other datasets. This phenomenon is mainly due to our method's emphasis on globally physically plausible motion rather than per-pixel overfitting.

Qualitative comparisons of visualization results. Figure 3 visually comparison results. On the "Bat" dataset, only ParticleGS and NVFi achieve motion trajectory estimates close to the ground truth. Our method captures wing vein details more clearly and demonstrates more stable extrapolation. In the more challenging "Chessboard" dataset, only ParticleGS can accurately localize the object and generate high-quality, visually recognizable renderings. See the Appendix for more visualization results.



Figure 3: Qualitative results of baselines and our method.

5.3 Ablation Study and Analysis

Table 4 presents the results of the ablation study. The results show that: 1) Removing the latent dynamics state leads to a significant performance drop, as the model relies on learning the dynamics of Gaussian particles in the latent space, which is crucial for capturing scene dynamics. 2) Removing either the Dynamics Evolution Module or the affine transformations also results in performance degradation, indicating that our proposed modules are effective in learning motion patterns.

6 Conclusion

We propose ParticalGS, a motion extrapolation model inspired by particle dynamics that requires no physical priors. By introducing dynamic latent states for Gaussian particles, it ensures stable extrapolation. Experiments show that ParticalGS matches SOTA performance in reconstruction and significantly outperforms them in extrapolation. A limitation of ParticalGS is its current reliance on specific training data, which may restrict its ability to fully capture generalizable motion patterns. Incorporating large-scale pretraining could address this, and future work will investigate this direction.

References

- [1] Yuqi Wang, Jiawei He, Lue Fan, Hongxin Li, Yuntao Chen, and Zhaoxiang Zhang. Driving into the future: Multiview visual forecasting and planning with world model for autonomous driving. In *Proceedings of the IEEE/CVF Conference on Computer Vision and Pattern Recognition*, pages 14749–14759, 2024.
- [2] Hang Yin, Anastasia Varava, and Danica Kragic. Modeling, learning, perception, and control methods for deformable object manipulation. *Science Robotics*, 6(54):eabd8803, 2021.
- [3] Shaojie Ma, Yawei Luo, and Yi Yang. Reconstructing and simulating dynamic 3d objects with mesh-adsorbed gaussian splatting. *arXiv preprint arXiv:2406.01593*, 2024.
- [4] Ziyi Yang, Xinyu Gao, Wen Zhou, Shaohui Jiao, Yuqing Zhang, and Xiaogang Jin. Deformable 3d gaussians for high-fidelity monocular dynamic scene reconstruction. In *Proceedings of the IEEE/CVF Conference on Computer Vision and Pattern Recognition*, pages 20331–20341, 2024.
- [5] Guanjin Wu, Taoran Yi, Jiemin Fang, Lingxi Xie, Xiaopeng Zhang, Wei Wei, Wenyu Liu, Qi Tian, and Xinggang Wang. 4d gaussian splatting for real-time dynamic scene rendering. In *Proceedings of the IEEE/CVF Conference on Computer Vision and Pattern Recognition*, pages 20310–20320, 2024.
- [6] Albert Pumarola, Enric Corona, Gerard Pons-Moll, and Francesc Moreno-Noguer. D-nerf: Neural radiance fields for dynamic scenes. In *Proceedings of the IEEE/CVF Conference on Computer Vision and Pattern Recognition*, pages 10318–10327, 2021.
- [7] Ang Cao and Justin Johnson. Hexplane: A fast representation for dynamic scenes. In *Proceedings of the IEEE/CVF Conference on Computer Vision and Pattern Recognition*, pages 130–141, 2023.
- [8] Jiawei Xu, Zexin Fan, Jian Yang, and Jin Xie. Grid4d: 4d decomposed hash encoding for high-fidelity dynamic gaussian splatting. In *Advances in Neural Information Processing Systems*.
- [9] Jiemin Fang, Taoran Yi, Xinggang Wang, Lingxi Xie, Xiaopeng Zhang, Wenyu Liu, Matthias Nießner, and Qi Tian. Fast dynamic radiance fields with time-aware neural voxels. In *SIGGRAPH Asia 2022 Conference Papers*, pages 1–9, 2022.
- [10] Qiaowei Miao, Kehan Li, Jinsheng Quan, Zhiyuan Min, Shaojie Ma, Yichao Xu, Yi Yang, and Yawei Luo. Advances in 4d generation: A survey. *arXiv preprint arXiv:2503.14501*, 2025.
- [11] Tianyi Xie, Zeshun Zong, Yuxing Qiu, Xuan Li, Yutao Feng, Yin Yang, and Chenfanfu Jiang. Physgaussian: Physics-integrated 3d gaussians for generative dynamics. In *Proceedings of the IEEE/CVF Conference on Computer Vision and Pattern Recognition*, pages 4389–4398, 2024.
- [12] Shanyan Guan, Huayu Deng, Yunbo Wang, and Xiaokang Yang. Neurofluid: Fluid dynamics grounding with particle-driven neural radiance fields. In *International Conference on Machine Learning*, pages 7919–7929, 2022.
- [13] Mengyu Chu, Lingjie Liu, Quan Zheng, Erik Franz, Hans-Peter Seidel, Christian Theobalt, and Rhaleb Zayer. Physics informed neural fields for smoke reconstruction with sparse data. *ACM Transactions on Graphics*, 41(4):1–14, 2022.
- [14] Junhao Cai, Yuji Yang, Weihao Yuan, HE Yisheng, Zilong Dong, Liefeng Bo, Hui Cheng, and Qifeng Chen. Gic: Gaussian-informed continuum for physical property identification and simulation. In *Advances in Neural Information Processing Systems*.
- [15] Yuchen Lin, Chenguo Lin, Jianjin Xu, and Yadong MU. OmniphysGS: 3d constitutive gaussians for general physics-based dynamics generation. In *Proceedings of the International Conference on Learning Representations*, 2025.
- [16] Xuan Li, Yi-Ling Qiao, Peter Yichen Chen, Krishna Murthy Jatavallabhula, Ming Lin, Chenfanfu Jiang, and Chuang Gan. Pac-nerf: Physics augmented continuum neural radiance fields for geometry-agnostic system identification. In *Proceedings of the International Conference on Learning Representations*, 2023.

- [17] Maziar Raissi, Paris Perdikaris, and George E Karniadakis. Physics-informed neural networks: A deep learning framework for solving forward and inverse problems involving nonlinear partial differential equations. *Journal of Computational physics*, 378:686–707, 2019.
- [18] Jinxi Li, Ziyang Song, and Bo Yang. Nvfi: Neural velocity fields for 3d physics learning from dynamic videos. *Advances in Neural Information Processing Systems*, 36:34723–34751, 2023.
- [19] Gilles Daviet, Tianchang Shen, Nicholas Sharp, and David IW Levin. Neurally integrated finite elements for differentiable elasticity on evolving domains. *ACM Transactions on Graphics*, 2024.
- [20] Chenfanfu Jiang, Craig Schroeder, Joseph Teran, Alexey Stomakhin, and Andrew Selle. The material point method for simulating continuum materials. In *Acm siggraph 2016 courses*, pages 1–52. 2016.
- [21] Sebastian Martin, Peter Kaufmann, Mario Botsch, Eitan Grinspun, and Markus Gross. Unified simulation of elastic rods, shells, and solids. *ACM Transactions on Graphics*, 29(4):1–10, 2010.
- [22] Yutao Feng, Yintong Shang, Xuan Li, Tianjia Shao, Chenfanfu Jiang, and Yin Yang. Pie-nerf: Physics-based interactive elastodynamics with nerf. In *Proceedings of the IEEE/CVF Conference on Computer Vision and Pattern Recognition*, pages 4450–4461, 2024.
- [23] Minghao Guo, Bohan Wang, Pingchuan Ma, Tianyuan Zhang, Crystal Owens, Chuang Gan, Josh Tenenbaum, Kaiming He, and Wojciech Matusik. Physically compatible 3d object modeling from a single image. *Advances in Neural Information Processing Systems*, 37:119260–119282, 2024.
- [24] Siwei Meng, Yawei Luo, and Ping Liu. Magic: Motion-aware generative inference via confidence-guided llm. *arXiv preprint arXiv:2505.16456*, 2025.
- [25] Ricky TQ Chen, Yulia Rubanova, Jesse Bettencourt, and David K Duvenaud. Neural ordinary differential equations. *Advances in Neural Information Processing Systems*, 31, 2018.
- [26] Michael Niemeyer, Lars Mescheder, Michael Oechsle, and Andreas Geiger. Occupancy flow: 4d reconstruction by learning particle dynamics. In *Proceedings of the IEEE/CVF International Conference on Computer Vision*, pages 5379–5389, 2019.
- [27] Boyan Jiang, Yinda Zhang, Xingkui Wei, Xiangyang Xue, and Yanwei Fu. Learning compositional representation for 4d captures with neural ode. In *Proceedings of the IEEE/CVF Conference on Computer Vision and Pattern Recognition*, pages 5340–5350, 2021.
- [28] Ben Mildenhall, Pratul P Srinivasan, Matthew Tancik, Jonathan T Barron, Ravi Ramamoorthi, and Ren Ng. Nerf: Representing scenes as neural radiance fields for view synthesis. *Communications of the ACM*, 65(1):99–106, 2021.
- [29] Sara Fridovich-Keil, Giacomo Meanti, Frederik Rahbæk Warburg, Benjamin Recht, and Angjoo Kanazawa. K-planes: Explicit radiance fields in space, time, and appearance. In *Proceedings of the IEEE/CVF Conference on Computer Vision and Pattern Recognition*, pages 12479–12488, 2023.
- [30] Nagabhushan Somraj, Kapil Choudhary, Sai Harsha Mupparaju, and Rajiv Soundararajan. Factorized motion fields for fast sparse input dynamic view synthesis. In *ACM SIGGRAPH 2024 Conference Papers*, pages 1–12, 2024.
- [31] Ruizhi Shao, Zerong Zheng, Hanzhang Tu, Boning Liu, Hongwen Zhang, and Yebin Liu. Tensor4d: Efficient neural 4d decomposition for high-fidelity dynamic reconstruction and rendering. In *Proceedings of the IEEE/CVF Conference on Computer Vision and Pattern Recognition*, pages 16632–16642, 2023.
- [32] Thomas Müller, Alex Evans, Christoph Schied, and Alexander Keller. Instant neural graphics primitives with a multiresolution hash encoding. *ACM transactions on graphics*, 41(4):1–15, 2022.

- [33] Feng Wang, Zilong Chen, Guokang Wang, Yafei Song, and Huaping Liu. Masked space-time hash encoding for efficient dynamic scene reconstruction. *Advances in neural information processing systems*, 36:70497–70510, 2023.
- [34] Chaoyang Wang, Lachlan Ewen MacDonald, Laszlo A Jeni, and Simon Lucey. Flow supervision for deformable nerf. In *Proceedings of the IEEE/CVF Conference on Computer Vision and Pattern Recognition*, pages 21128–21137, 2023.
- [35] Xiang Guo, Jiadai Sun, Yuchao Dai, Guanying Chen, Xiaoqing Ye, Xiao Tan, Errui Ding, Yumeng Zhang, and Jingdong Wang. Forward flow for novel view synthesis of dynamic scenes. In *Proceedings of the IEEE/CVF International Conference on Computer Vision*, pages 16022–16033, 2023.
- [36] Zhiwen Yan, Chen Li, and Gim Hee Lee. Nerf-ds: Neural radiance fields for dynamic specular objects. In *Proceedings of the IEEE/CVF Conference on Computer Vision and Pattern Recognition*, pages 8285–8295, 2023.
- [37] Bernhard Kerbl, Georgios Kopanas, Thomas Leimkühler, and George Drettakis. 3d gaussian splatting for real-time radiance field rendering. *ACM TRANSACTIONS ON GRAPHICS*, 42(4):139–1, 2023.
- [38] Jonathon Luiten, Georgios Kopanas, Bastian Leibe, and Deva Ramanan. Dynamic 3d gaussians: Tracking by persistent dynamic view synthesis. In *International Conference on 3D Vision*, pages 800–809. IEEE, 2024.
- [39] Agelos Kratimenos, Jiahui Lei, and Kostas Daniilidis. Dynmf: Neural motion factorization for real-time dynamic view synthesis with 3d gaussian splatting. In *European Conference on Computer Vision*, pages 252–269. Springer, 2024.
- [40] Yi-Hua Huang, Yang-Tian Sun, Ziyi Yang, Xiaoyang Lyu, Yan-Pei Cao, and Xiaojuan Qi. Sc-gs: Sparse-controlled gaussian splatting for editable dynamic scenes. In *Proceedings of the IEEE/CVF Conference on computer Vision and Pattern Recognition*, pages 4220–4230, 2024.
- [41] Jiakai Sun, Han Jiao, Guangyuan Li, Zhanjie Zhang, Lei Zhao, and Wei Xing. 3dgsstream: On-the-fly training of 3d gaussians for efficient streaming of photo-realistic free-viewpoint videos. In *Proceedings of the IEEE/CVF Conference on Computer Vision and Pattern Recognition*, pages 20675–20685, 2024.
- [42] Priya Sundaesan, Rika Antonova, and Jeannette Bohgl. Diffcloud: Real-to-sim from point clouds with differentiable simulation and rendering of deformable objects. In *International Conference on Intelligent Robots and Systems*, pages 10828–10835. IEEE, 2022.
- [43] Junbang Liang, Ming Lin, and Vladlen Koltun. Differentiable cloth simulation for inverse problems. *Advances in neural information processing systems*, 32, 2019.
- [44] Licheng Zhong, Hong-Xing Yu, Jiajun Wu, and Yunzhu Li. Reconstruction and simulation of elastic objects with spring-mass 3d gaussians. In *European Conference on Computer Vision*, pages 407–423. Springer, 2024.
- [45] Siwei Meng, Yawei Luo, and Ping Liu. Grounding creativity in physics: A brief survey of physical priors in aigc. *arXiv preprint arXiv:2502.07007*, 2025.
- [46] Donglai Xiang, Timur Bagautdinov, Tuur Stuyck, Fabian Prada, Javier Romero, Weipeng Xu, Shunsuke Saito, Jingfan Guo, Breannan Smith, Takaaki Shiratori, et al. Dressing avatars: Deep photorealistic appearance for physically simulated clothing. *ACM Transactions on Graphics*, 41(6):1–15, 2022.
- [47] Chenfanfu Jiang, Theodore Gast, and Joseph Teran. Anisotropic elastoplasticity for cloth, knit and hair frictional contact. *ACM Transactions on Graphics*, 36(4):1–14, 2017.
- [48] Salvatore Cuomo, Vincenzo Schiano Di Cola, Fabio Giampaolo, Gianluigi Rozza, Maziar Raissi, and Francesco Piccialli. Scientific machine learning through physics-informed neural networks: Where we are and what’s next. *Journal of Scientific Computing*, 92(3):88, 2022.

- [49] Ramansh Sharma and Varun Shankar. Accelerated training of physics-informed neural networks (pinns) using meshless discretizations. *Advances in neural information processing systems*, 35:1034–1046, 2022.
- [50] Yawei Luo and Yi Yang. Large language model and domain-specific model collaboration for smart education. *Frontiers of Information Technology & Electronic Engineering*, 25(3):333–341, 2024.
- [51] Tianyuan Zhang, Hong-Xing Yu, Rundi Wu, Brandon Y Feng, Changxi Zheng, Noah Snively, Jiajun Wu, and William T Freeman. Physdreamer physics-based interaction with 3d objects via video generation. In *European Conference on Computer Vision*, pages 388–406. Springer, 2024.
- [52] Filipe de Avila Belbute-Peres, Kevin Smith, Kelsey Allen, Josh Tenenbaum, and J Zico Kolter. End-to-end differentiable physics for learning and control. *Advances in neural information processing systems*, 31, 2018.
- [53] Yifei Li, Hsiao-yu Chen, Egor Larionov, Nikolaos Sarafianos, Wojciech Matusik, and Tuur Stuyck. Diffavatar: Simulation-ready garment optimization with differentiable simulation. In *Proceedings of the IEEE/CVF Conference on Computer Vision and Pattern Recognition*, pages 4368–4378, 2024.
- [54] Tao Du, Kui Wu, Pingchuan Ma, Sebastien Wah, Andrew Spielberg, Daniela Rus, and Wojciech Matusik. Diffpd: Differentiable projective dynamics. *ACM Transactions on Graphics*, 41(2):1–21, 2021.
- [55] Junbang Liang and Ming C Lin. Differentiable physics simulation. In *ICLR 2020 Workshop on Integration of Deep Neural Models and Differential Equations*, 2020.
- [56] Boming Zhao, Yuan Li, Ziyu Sun, Lin Zeng, Yujun Shen, Rui Ma, Yinda Zhang, Hujun Bao, and Zhaopeng Cui. Gaussianprediction: Dynamic 3d gaussian prediction for motion extrapolation and free view synthesis. In *ACM SIGGRAPH 2024 Conference Papers*, pages 1–12, 2024.
- [57] Jiaqi Han, Wenbing Huang, Hengbo Ma, Jiachen Li, Josh Tenenbaum, and Chuang Gan. Learning physical dynamics with subequivariant graph neural networks. *Advances in Neural Information Processing Systems*, 35:26256–26268, 2022.
- [58] Alvaro Sanchez-Gonzalez, Jonathan Godwin, Tobias Pfaff, Rex Ying, Jure Leskovec, and Peter Battaglia. Learning to simulate complex physics with graph networks. In *International conference on machine learning*, pages 8459–8468. PMLR, 2020.
- [59] Charles R Qi, Hao Su, Kaichun Mo, and Leonidas J Guibas. Pointnet: Deep learning on point sets for 3d classification and segmentation. In *Proceedings of the IEEE conference on Computer Vision and Pattern Recognition*, pages 652–660, 2017.
- [60] Xumin Yu, Lulu Tang, Yongming Rao, Tiejun Huang, Jie Zhou, and Jiwen Lu. Point-bert: Pre-training 3d point cloud transformers with masked point modeling. In *Proceedings of the IEEE/CVF conference on Computer Vision and Pattern Recognition*, pages 19313–19322, 2022.
- [61] Keunhong Park, Utkarsh Sinha, Peter Hedman, Jonathan T Barron, Sofien Bouaziz, Dan B Goldman, Ricardo Martin-Brualla, and Steven M Seitz. Hypernerf: a higher-dimensional representation for topologically varying neural radiance fields. *ACM Transactions on Graphics*, 40(6):1–12, 2021.

A Appendix

The appendix includes:

- Implementation details of ParticleGS.
- Limitations.
- Additional quantitative results for future frame extrapolation.

A.1 Implementation details of ParticleGS

Dynamics Latent Space Encoder. For local feature encoding, the upper bound of the hash table size is set to 2^{19} . For all grids, the feature dimension of each voxel is 2. We adopt the same parameter settings for both synthetic and real-world datasets. For global feature encoding, we use a standard 4-layer transformer block with 4 decoding heads. All datasets use the same number of FPS center points and neighborhood groups.

Neural ODEs Dynamics Evolution Module. We employ a 1-layer ODE module with a width of 256, using the commonly adopted RK4 numerical integration method in physical simulations.

Gaussian Kernel Space Decoder. We use MLPs with a width of 256 and depths of 4 and 5 as the multi-head decoders for motion and appearance, respectively. To ensure that the motion decoding is stable and physically plausible, we first decompose the affine transformation matrix A and translation b into components such as rotation, scaling, shearing, linear velocity, and nonlinear terms. These components are further decomposed into direction and magnitude.

Optimization. We set $\lambda = 0.2$. The number of warm-up is 3,000 steps, the training steps is 50,000 for the Dynamic Object Dataset, 60,000 for the Dynamic Indoor Scene Dataset, and 80,000 for the real-world dataset. The background is set to black.

A.2 Limitations

Although new scene generalization is a challenging problem due to the high-frequency features of object textures, motion generalization often follows similar patterns. Since the global feature encoding used in this work is inspired by the designs of PointNet and Point-BERT, we believe that the proposed method has the potential to generalize to object motion in new scenes after large-scale pretraining. However, due to limitations in the dataset and computational resources, we did not conduct further exploration in this direction, which is a major limitation of this work. We plan to investigate this further in the future.

A.3 Additional quantitative results for future frame extrapolation

Due to the high complexity of the PanopticSports dataset, even state-of-the-art reconstruction algorithms are unable to render high-quality human motion details without incorporating additional priors. However, since Gaussian particles carry color information, this does not affect the ability of quantitative metrics such as PSNR, SSIM, and LPIPS to reflect the motion of Gaussian particles. Therefore, we do not perform a qualitative comparison in this case and instead focus solely on quantitative metrics. The figures below present some qualitative results on other datasets:

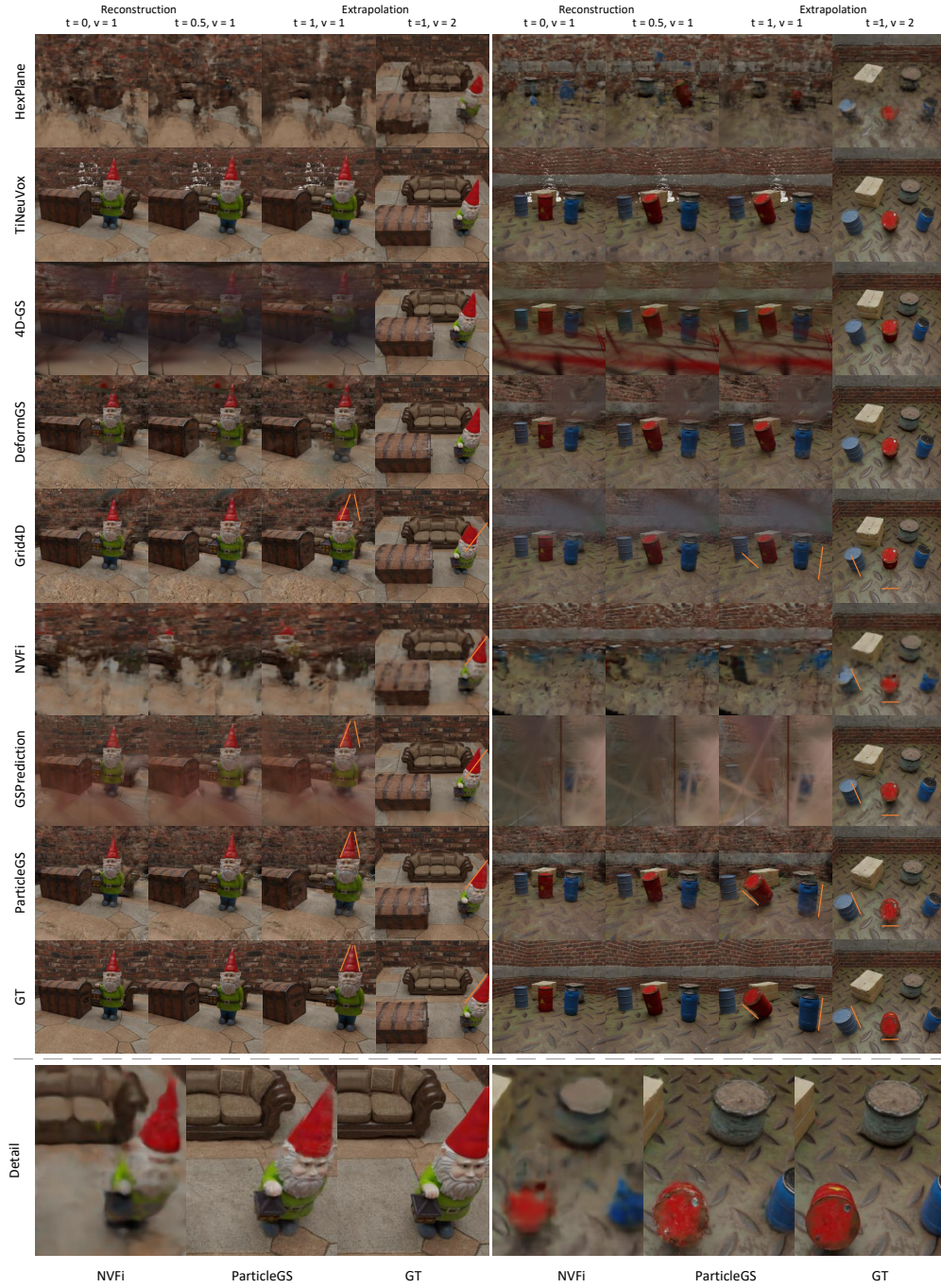


Figure 4: Qualitative results of prior arts and our method.



Figure 5: Qualitative results of prior arts and our method.

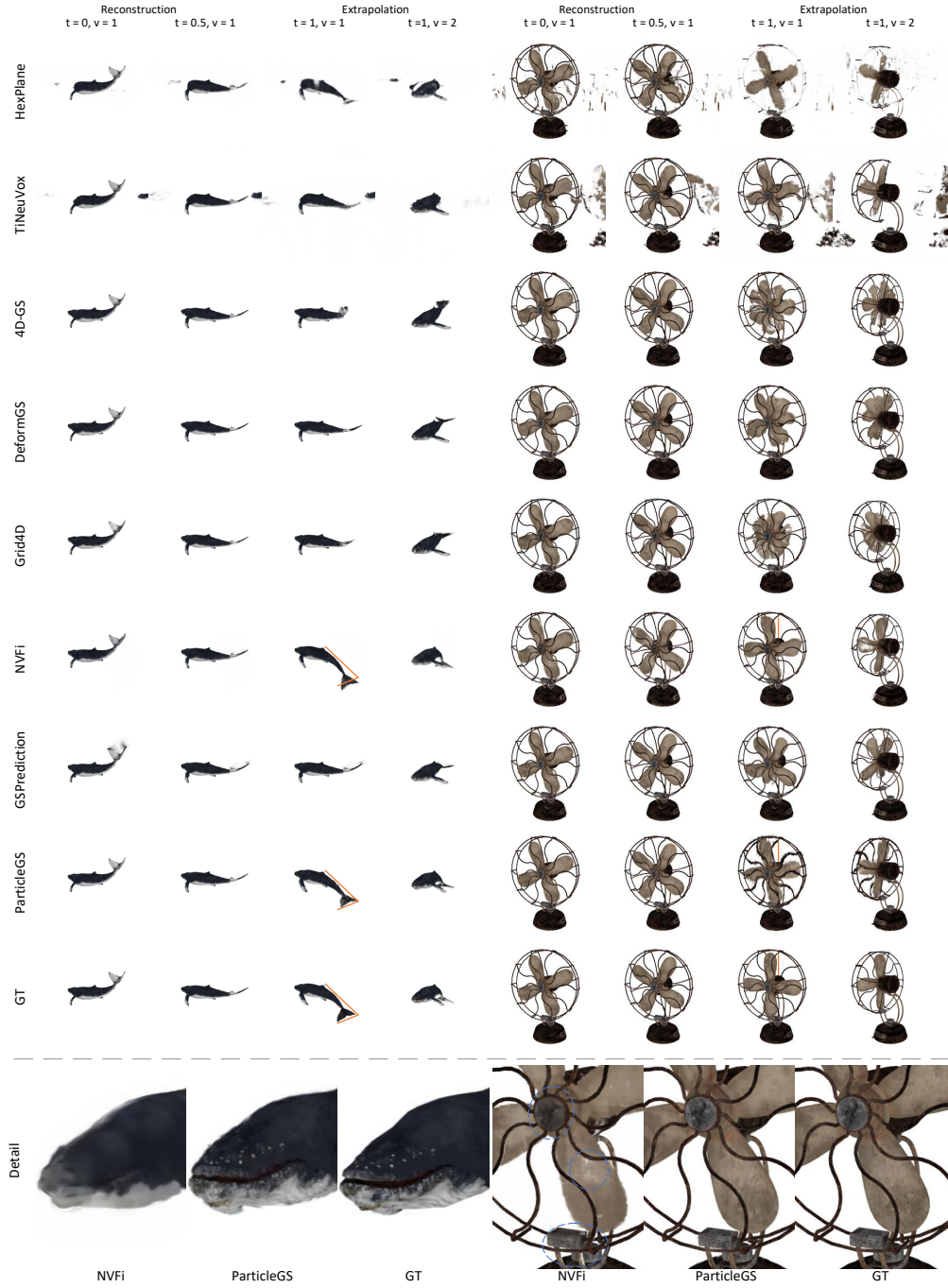


Figure 6: Qualitative results of prior arts and our method.